NCCE29

From Knowledge to Transformation

CONFERENCE PROCEEDINGS

การประชุมวิชาการ วิศวกรรมโยธาแห่งชาติ ครั้งที่ 29

The 29th National Convention on Civil Engineering

"จากภูมิปัญญาที่สืบสานสู่การรังสรรค์โลกที่ยั่งยืน"
(From Knowledge to Transformation)

วันที่ 29 - 31 พฤษภาคม 2567
ณ ศูนย์ประชุมนานาชาติดิเอ็มเพรส จังหวัดเชียงใหม่

จัดประชุมโดย

มหาวิทยาลัยธรรมศาสตร์ THAMMASAT UNIVERSITY

TSE

Nonlinear Free Vibration Analysis of a Novel Reinforced Functionally Graded Plate via Refined Plate Theory

Sunchhorng Roun[1,*] Van-Loi Nguyen[2] and Jaroon Rungamornrat[3]

[1]Department of Civil Environmental and Sustainable Engineering, Faculty of Engineering, Siam University, Bangkok, THAILAND
[2]Department of Strength of Materials, Hanoi University of Civil Engineering, Hanoi, VIETNAM
[3]Center of Excellence in Applied Mechanics and Structures, Department of Civil Engineering, Faculty of Engineering, Chulalongkorn University, Bangkok, THAILAND
**Corresponding author; E-mail address: sunchhorng.roun@siam.edu*

Abstract

This research presents a nonlinear free vibration analysis of an advanced nanocomposite plate consisting of a functionally graded matrix reinforced by graphene platelets (GPLs), which is a novel technique to enhance the stiffness of plate structures. The matrix phase's constituent materials exhibit continuous gradation according to the power law distribution across the plate's thickness, and several GPL dispersion patterns are investigated. The equations of motion are constructed based on Hamilton's principle through the utilization of the four-unknown refined plate theory (RPT4), the physical neutral surface theory, and von Karman's geometric nonlinearity. The Bubnov-Galerkin method and variational approach are then employed to calculate closed-form solutions for the natural frequency. Following that, various parametric studies are also conducted.

Keywords: Nonlinear Free Vibration, Functionally Graded Matrix, Graphene Platelets, Refined Plate Theory

1. Introduction

Functionally graded materials (FGMs) have become a popular research topic due to their superior performance compared to conventional materials, effective prevention of interfacial cracking, ability to fulfill multiple performance criteria, and potential for innovative lightweight structures [1, 2]. Since their introduction in 1984, there have been numerous studies on the dynamic behavior of functionally graded (FG) plates, including static and dynamic responses [3], nonlinear vibrations in thermal environments using higher-order shear deformation theory and von Karman's nonlinearity [4-7], and experimental and numerical investigations of geometrically nonlinear vibrations [8].

Advancements in nanotechnology have enabled the creation of nanocomposites by integrating carbon nanomaterials like graphene platelets (GPLs) into polymer, ceramic, and metal matrices, resulting in exceptional mechanical, thermal, and electrical properties [9-11]. GPLs, consisting of a 2D honeycomb arrangement of carbon atoms, exhibit remarkable properties like high elastic modulus, tensile strength, and large specific surface area, surpassing even carbon nanotubes [12, 13]. Studies have shown that adding GPLs significantly enhances the flexural strength and fracture toughness of alumina [14] and silicon carbide [15] ceramic composites, as well as the yield strength and compressive strength of titanium composites for high-temperature applications [16]. Investigations on nanocomposite plates with functionally graded GPLs/polymer have observed a notable increase in stiffness due to GPL reinforcement [17, 18].

The Increasing utilization of FG plates in engineering structures is often subjected to vibrations. To model the plate vibrations, many plate theories have been developed, including classical plate theory, first-order shear deformation theory requiring a shear correction factor, and higher-order shear deformation theories to eliminate the need for a correction factor. The four-unknown refined plate theory (RPT4) simplifies the higher-order shear deformation theories while sharing similarities with the classical plate theory's governing equations.

The asymmetrical material property distribution in FG plates can cause the physical neutral surface to deviate from the geometric neutral surface, resulting in a stretching-bending

coupling effect that can be mitigated by employing the physical neutral surface concept [19-23].

This study aims to investigate the nonlinear free vibration analysis of plate structures made of FG matrix reinforced by GPLs based on the physical neutral surface concept and RPT4. The governing equations that describe the motion of the plate model are established using Hamilton's principle. To approximately solve for the nonlinear vibration frequency, the authors employ the Bubnov-Galerkin technique along with a variational approach. These mathematical methods allow us to derive closed-form expressions that capture the nonlinear vibration behavior. Additionally, the study also explores the influence of various parameters on the nonlinear frequency of a rectangular nanocomposite plate.

2. Problem Formulation

2.1 Descriptions Of The Plate Model

The analysis focuses on a nanocomposite plate depicted in Fig. 1. With a uniform thickness h across its entire area, the plate model has dimensions of length a and width b. The boundary conditions are such that all four edges are simply supported, allowing no movement in the normal direction but free movement along the tangential direction. The nanocomposite plate comprises three distinct materials: two constituent materials of the matrix phase (a ceramic and a metal), as well as the GPL nanofiller serving as the reinforcement of the plate.

2.2 Constitutive Modeling of Nanocomposite

The volume fractions V of the matrix constituents (ceramic and metal) varying continuously through the thickness of the plate by a power law function, and Young's modulus E_M and mass density ρ_M of the FG matrix provided by the rule of mixture are expressed as:

$$V_1(z)=\left(\frac{z}{h}+\frac{1}{2}\right)^N, V_2(z)=1-V_1(z), z\in\left[-\frac{h}{2},\frac{h}{2}\right], \quad (1)$$

$$E_M(z)=(E_1-E_2)\left(\frac{z}{h}+\frac{1}{2}\right)^N+E_2, \quad (2)$$

$$\rho_M(z)=(\rho_1-\rho_2)\left(\frac{z}{h}+\frac{1}{2}\right)^N+\rho_2, \quad (3)$$

where the power law index N indicates the distribution pattern of the volume fraction of these constituent materials, while the subscripts *"1"* and *"2"* represent the constituents of the FG matrix (ceramic and metal, respectively).

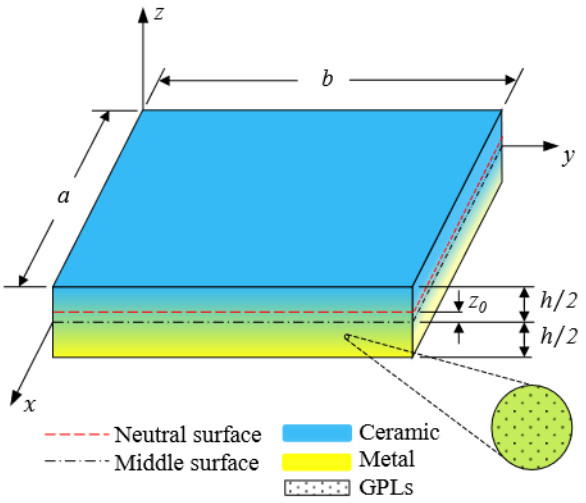

Fig. 1 A functionally graded plate reinforced by GPLs.

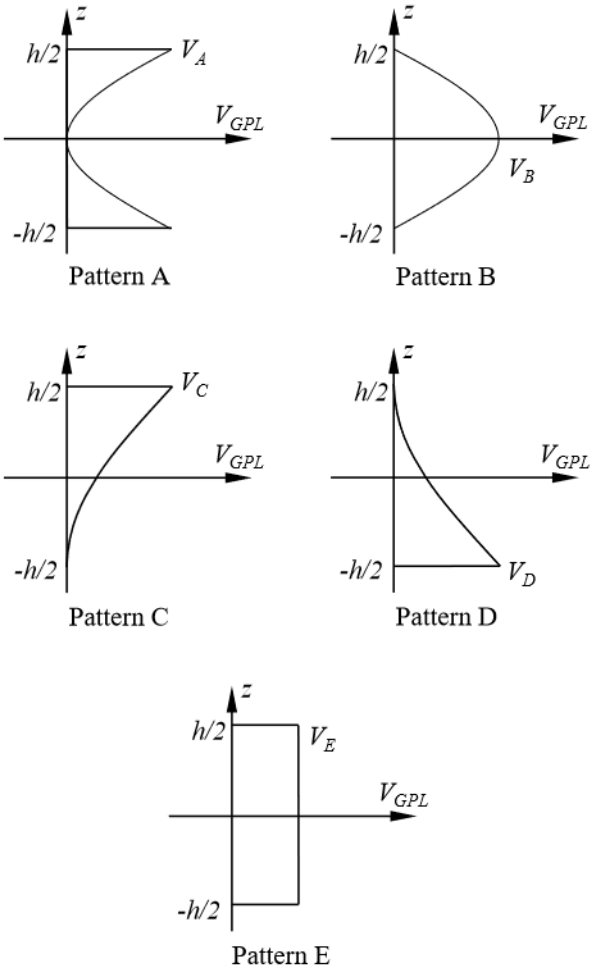

Fig. 2 GPL dispersion patterns.

The volume fraction of GPL in each distribution pattern, as depicted in Fig. 2, assumed to vary along the z-axis smoothly, can be introduced as:

$$V_{GPL}(z)=\begin{Bmatrix}V_A\psi_A\\V_B\psi_B\\V_C\psi_C\\V_D\psi_D\\V_E\psi_E\end{Bmatrix},\begin{Bmatrix}\psi_A\\\psi_B\\\psi_C\\\psi_D\\\psi_E\end{Bmatrix}=\begin{Bmatrix}1-\cos\left(\frac{\pi z}{h}\right)\\\cos\left(\frac{\pi z}{h}\right)\\1-\cos\left(\frac{\pi z}{2h}+\frac{\pi}{4}\right)\\1-\cos\left(\frac{\pi z}{2h}-\frac{\pi}{4}\right)\\1\end{Bmatrix}, \quad (4)$$

where the maximum volume fractions of patterns A, B, C, D, and E, denoted as V_A, V_B, V_C, V_D, and V_E, respectively, are determined based on the total weight fraction of GPLs to ensure that the total amount of GPLs remains constant across all patterns as follows [24]:

$$V_i=\frac{W_{GPL}k_{2i}}{W_{GPL}k_{3i}+\rho_{GPL}k_{1i}\left(1-W_{GPL}\right)}, \quad (5)$$

$$k_{1i}=\int_{-h/2}^{h/2}\psi_i(z)dz,\qquad k_{2i}=\int_{-h/2}^{h/2}\rho_M(z)dz,$$
$$k_{3i}=\int_{-h/2}^{h/2}\rho_M(z)\psi_i(z)dz \quad (6)$$

where $i=A,B,C,D,$ and E represent the GPLs dispersion patterns. W_{GPL} and ρ_{GPL} are the weight fraction and density of the GPLs, respectively.

According to Halpin-Tsai model, the Young's modulus of the composite made of randomly oriented fillers is given by [2, 25]:

$$E(z)=\frac{3}{8}\frac{1+\xi_{11}\eta_{11}V_{GPL}}{1-\eta_{11}V_{GPL}}E_M+\frac{5}{8}\frac{1+\xi_{22}\eta_{22}V_{GPL}}{1-\eta_{22}V_{GPL}}E_M, \quad (7)$$

$$\eta_{11}=\frac{(E_{GPL}/E_M)-1}{(E_{GPL}/E_M)+\xi_{11}},\eta_{22}=\frac{(E_{GPL}/E_M)-1}{(E_{GPL}/E_M)+\xi_{22}} \quad (8)$$

$$\xi_{11}=2l_f/t_f,\xi_{22}=2w_f/t_f, \quad (9)$$

where l_f, w_f, t_f, and d_f are the average length, width, thickness, and diameter of the filler (GPLs), respectively. In this work, the Poisson's ratio ν of the nanocomposite will be assumed to remain constant, and the mass density ρ of the whole plate is given by the ROM as:

$$\rho(z)=\rho_{GPL}V_{GPL}(z)+\rho_MV_M(z), \quad (10)$$

where $V_M(z)=1-V_{GPL}(z)$ is the volume fraction of the FG matrix.

2.3 The refined plate theory and neutral surface position

As depicted in Fig. 1, the physical neutral surface is defined at $z=z_0$. With this reference plane, the displacement fields of the FG nanocomposite according to the general form of RPT are expressed as[26, 27]:

$$u_1(x,y,z,t)=u(x,y,t)-(z-z_0)\frac{\partial w_b}{\partial x}-\left[f(z)-z_1\right]\frac{\partial w_s}{\partial x},$$
$$u_2(x,y,z,t)=v(x,y,t)-(z-z_0)\frac{\partial w_b}{\partial y}-\left[f(z)-z_1\right]\frac{\partial w_s}{\partial y}, \quad (11)$$
$$u_3(x,y,z,t)=w_b(x,y,t)+w_s(x,y,t),$$

where u_1, u_2, and u_3, respectively, stand for the displacements in the x, y, and z directions. The displacement components of the plate in the x and y directions are denoted by u and v. The transverse displacement u_3 consists of the bending component w_b and the shear component w_s. In this work, the selected shape function to describe the transverse shear deformation is defined as $f(z)=-z/4+5z^3/(3h^2)$. To take in account the physical neutral surface, z_0 and z_1 are defined by [26, 28]:

$$z_0=\frac{\int_{-h/2}^{h/2}E(z)zdz}{\int_{-h/2}^{h/2}E(z)dz},z_1=\frac{\int_{-h/2}^{h/2}E(z)f(z)dz}{\int_{-h/2}^{h/2}E(z)dz}. \quad (12)$$

The strain field with considering the Von Karman's nonlinearity can be obtained as:

$$\begin{Bmatrix}\varepsilon_x\\\varepsilon_y\\\gamma_{xy}\end{Bmatrix}=\begin{Bmatrix}\varepsilon_x^0\\\varepsilon_y^0\\\gamma_{xy}^0\end{Bmatrix}+(z-z_0)\begin{Bmatrix}k_x^b\\k_y^b\\k_{xy}^b\end{Bmatrix}+\left[f(z)-z_1\right]\begin{Bmatrix}k_x^s\\k_y^s\\k_{xy}^s\end{Bmatrix},$$
$$\begin{Bmatrix}\gamma_{xz}\\\gamma_{yz}\end{Bmatrix}=g(z)\begin{Bmatrix}\gamma_{xz}^s\\\gamma_{yz}^s\end{Bmatrix}. \quad (13)$$

in which

$$\begin{Bmatrix}\varepsilon_x^0\\\varepsilon_y^0\\\gamma_{xy}^0\end{Bmatrix}=\begin{Bmatrix}\frac{\partial u}{\partial x}+\frac{1}{2}\left(\frac{\partial w_b}{\partial x}+\frac{\partial w_s}{\partial x}\right)^2\\\frac{\partial v}{\partial y}+\frac{1}{2}\left(\frac{\partial w_b}{\partial y}+\frac{\partial w_s}{\partial y}\right)^2\\\frac{\partial u}{\partial y}+\frac{\partial v}{\partial x}+\left(\frac{\partial w_b}{\partial x}+\frac{\partial w_s}{\partial x}\right)\left(\frac{\partial w_b}{\partial y}+\frac{\partial w_s}{\partial y}\right)\end{Bmatrix},$$
$$\begin{Bmatrix}k_x^b\\k_y^b\\k_{xy}^b\end{Bmatrix}=\begin{Bmatrix}-\frac{\partial^2 w_b}{\partial x^2}\\-\frac{\partial^2 w_b}{\partial y^2}\\-2\frac{\partial^2 w_b}{\partial x\partial y}\end{Bmatrix},\begin{Bmatrix}k_x^s\\k_y^s\\k_{xy}^s\end{Bmatrix}=\begin{Bmatrix}-\frac{\partial^2 w_s}{\partial x^2}\\-\frac{\partial^2 w_s}{\partial y^2}\\-2\frac{\partial^2 w_s}{\partial x\partial y}\end{Bmatrix}, \quad (14)$$
$$\begin{Bmatrix}\gamma_{xz}^s\\\gamma_{yz}^s\end{Bmatrix}=\begin{Bmatrix}\frac{\partial w_s}{\partial x}\\\frac{\partial w_s}{\partial y}\end{Bmatrix},g(z)=1-\frac{df}{dz}.$$

The material behavior of the plate model can be described by linear constitutive equations as follows:

$$\begin{Bmatrix}\sigma_x\\ \sigma_y\\ \sigma_{xy}\\ \sigma_{yz}\\ \sigma_{xz}\end{Bmatrix}=\frac{E(z)}{1-\nu^2}\begin{bmatrix}1 & \nu & 0 & 0 & 0\\ \nu & 1 & 0 & 0 & 0\\ 0 & 0 & \frac{1-\nu}{2} & 0 & 0\\ 0 & 0 & 0 & \frac{1-\nu}{2} & 0\\ 0 & 0 & 0 & 0 & \frac{1-\nu}{2}\end{bmatrix}\begin{Bmatrix}\varepsilon_x\\ \varepsilon_y\\ \gamma_{xy}\\ \gamma_{yz}\\ \gamma_{xz}\end{Bmatrix}. \tag{15}$$

2.4 Equations of motion

The equations of motion can be obtained using Hamilton's principle as follows:

$$\begin{aligned}
&\delta u:\frac{\partial N_x}{\partial x}+\frac{\partial N_{xy}}{\partial y}=I_0\ddot{u}-I_1\frac{\partial\ddot{w}_b}{\partial x}-I_3\frac{\partial\ddot{w}_s}{\partial x},\\
&\delta v:\frac{\partial N_{xy}}{\partial x}+\frac{\partial N_y}{\partial y}=I_0\ddot{v}-I_1\frac{\partial\ddot{w}_b}{\partial y}-I_3\frac{\partial\ddot{w}_s}{\partial y},\\
&\delta w_b:\frac{\partial^2 M_x^b}{\partial x^2}+2\frac{\partial^2 M_{xy}^b}{\partial x\partial y}+\frac{\partial^2 M_y^b}{\partial y^2}+\bar{N}=I_0\left(\ddot{w}_b+\ddot{w}_s\right)\\
&+I_1\left(\frac{\partial\ddot{u}}{\partial x}+\frac{\partial\ddot{v}}{\partial y}\right)-I_2\nabla^2\ddot{w}_b-J_1\nabla^2\ddot{w}_s,\\
&\delta w_s:\frac{\partial^2 M_x^s}{\partial x^2}+2\frac{\partial^2 M_{xy}^s}{\partial x\partial y}+\frac{\partial^2 M_y^s}{\partial y^2}+\frac{\partial Q_{xz}}{\partial x}+\frac{\partial Q_{yz}}{\partial y}\\
&+\bar{N}=I_0\left(\ddot{w}_b+\ddot{w}_s\right)+I_3\left(\frac{\partial\ddot{u}}{\partial x}+\frac{\partial\ddot{v}}{\partial y}\right)-J_1\nabla^2\ddot{w}_b-J_2\nabla^2\ddot{w}_s,
\end{aligned} \tag{16}$$

where

$$\bar{N}=\frac{\partial}{\partial x}\left(N_x\frac{\partial w}{\partial x}+N_{xy}\frac{\partial w}{\partial y}\right)+\frac{\partial}{\partial y}\left(N_y\frac{\partial w}{\partial y}+N_{xy}\frac{\partial w}{\partial x}\right). \tag{17}$$

The inertia related terms are expressed as:

$$\begin{Bmatrix}I_0\\ I_1\\ I_2\\ I_3\\ J_1\\ J_2\end{Bmatrix}=\int_{-h/2}^{h/2}\rho(z)\begin{Bmatrix}1\\ z-z_0\\ (z-z_0)^2\\ f(z)-z_1\\ (z-z_0)\left[f(z)-z_1\right]\\ \left[f(z)-z_1\right]^2\end{Bmatrix}dz. \tag{18}$$

The expression of stress resultants can be obtained as:

$$\begin{Bmatrix}N_x\\ N_y\\ N_{xy}\end{Bmatrix}=A\begin{bmatrix}1 & \nu & 0\\ \nu & 1 & 0\\ 0 & 0 & (1-\nu)/2\end{bmatrix}\begin{Bmatrix}\varepsilon_x^0\\ \varepsilon_y^0\\ \gamma_{xy}^0\end{Bmatrix}, \tag{19}$$

$$\begin{Bmatrix}M_x^b\\ M_y^b\\ M_{xy}^b\end{Bmatrix}=B\begin{bmatrix}1 & \nu & 0\\ \nu & 1 & 0\\ 0 & 0 & \frac{1-\nu}{2}\end{bmatrix}\begin{Bmatrix}k_x^b\\ k_y^b\\ k_{xy}^b\end{Bmatrix}+C\begin{bmatrix}1 & \nu & 0\\ \nu & 1 & 0\\ 0 & 0 & \frac{1-\nu}{2}\end{bmatrix}\begin{Bmatrix}k_x^s\\ k_y^s\\ k_{xy}^s\end{Bmatrix},$$

$$\begin{Bmatrix}M_x^s\\ M_y^s\\ M_{xy}^s\end{Bmatrix}=C\begin{bmatrix}1 & \nu & 0\\ \nu & 1 & 0\\ 0 & 0 & \frac{1-\nu}{2}\end{bmatrix}\begin{Bmatrix}k_x^b\\ k_y^b\\ k_{xy}^b\end{Bmatrix}+D\begin{bmatrix}1 & \nu & 0\\ \nu & 1 & 0\\ 0 & 0 & \frac{1-\nu}{2}\end{bmatrix}\begin{Bmatrix}k_x^s\\ k_y^s\\ k_{xy}^s\end{Bmatrix},$$

$$\begin{Bmatrix}Q_{xz}\\ Q_{yz}\end{Bmatrix}=A^s\begin{pmatrix}1 & 0\\ 0 & 1\end{pmatrix}\begin{Bmatrix}\gamma_{xz}^s\\ \gamma_{yz}^s\end{Bmatrix},$$

in which

$$\begin{aligned}
&A=\int_{-h/2}^{h/2}\frac{E(z)}{1-\nu^2}dz,B=\int_{-h/2}^{h/2}\frac{E(z)(z-z_0)^2}{1-\nu^2}dz,\\
&C=\int_{-h/2}^{h/2}\frac{E(z)(z-z_0)\left[f(z)-z_1\right]}{1-\nu^2}dz,\\
&D=\int_{-h/2}^{h/2}\frac{E(z)\left[f(z)-z_1\right]^2}{1-\nu^2}dz,\\
&A^s=\int_{-h/2}^{h/2}\frac{E(z)}{2(1+\nu)}g^2(z)dz.
\end{aligned} \tag{20}$$

Thus, the equations of motion based on nonlinear four-variable plate theory can be expressed in terms of displacements (u,v,w_b,w_s) as follows:

$$\begin{aligned}
&A\left(\frac{\partial^2 u}{\partial x^2}+\frac{1-\nu}{2}\frac{\partial^2 u}{\partial y^2}+\frac{1+\nu}{2}\frac{\partial^2 v}{\partial x\partial y}\right)\\
&+A\left(\frac{\partial w}{\partial x}\frac{\partial^2 w}{\partial x^2}+\frac{1-\nu}{2}\frac{\partial w}{\partial x}\frac{\partial^2 w}{\partial y^2}+\frac{1+\nu}{2}\frac{\partial w}{\partial y}\frac{\partial^2 w}{\partial x\partial y}\right)\\
&=I_0\ddot{u}-I_1\frac{\partial\ddot{w}_b}{\partial x}-I_3\frac{\partial\ddot{w}_s}{\partial x},
\end{aligned} \tag{21}$$

$$\begin{aligned}
&A\left(\frac{\partial^2 v}{\partial y^2}+\frac{1-\nu}{2}\frac{\partial^2 v}{\partial x^2}+\frac{1+\nu}{2}\frac{\partial^2 u}{\partial x\partial y}\right)\\
&+A\left(\frac{\partial w}{\partial y}\frac{\partial^2 w}{\partial y^2}+\frac{1-\nu}{2}\frac{\partial w}{\partial y}\frac{\partial^2 w}{\partial x^2}+\frac{1+\nu}{2}\frac{\partial w}{\partial x}\frac{\partial^2 w}{\partial x\partial y}\right)\\
&=I_0\ddot{v}-I_1\frac{\partial\ddot{w}_b}{\partial y}-I_3\frac{\partial\ddot{w}_s}{\partial y},
\end{aligned} \tag{22}$$

$$\begin{aligned}
&-D\nabla^4 w_b-E\nabla^4 w_s+\bar{N}=I_0\left(\ddot{w}_b+\ddot{w}_s\right)\\
&+I_1\left(\frac{\partial\ddot{u}}{\partial x}+\frac{\partial\ddot{v}}{\partial y}\right)-I_2\nabla^2\ddot{w}_b-J_1\nabla^2\ddot{w}_s,
\end{aligned} \tag{23}$$

$$\begin{aligned}
&-E\nabla^4 w_b-F\nabla^4 w_s+A^s\nabla^2 w_s+\bar{N}=I_0\left(\ddot{w}_b+\ddot{w}_s\right)\\
&+I_3\left(\frac{\partial\ddot{u}}{\partial x}+\frac{\partial\ddot{v}}{\partial y}\right)-J_1\nabla^2\ddot{w}_b-J_2\nabla^2\ddot{w}_s.
\end{aligned} \tag{24}$$

In the present work, $I_0, I_1,$ and I_3 are neglected for their relatively small contributions [29, 30].

3. Solution Procedure

The assumed forms of displacements (u, v, w_s, w_b) are as follows[31]:

$$\begin{aligned} u(x,y,t) &= \frac{\alpha}{16} W_{mn}^2(t)\sin(2\alpha x)\left[\cos(2\beta y)-1+\nu\frac{\beta^2}{\alpha^2}\right], \\ v(x,y,t) &= \frac{\beta}{16} W_{mn}^2(t)\sin(2\beta y)\left[\cos(2\alpha x)-1+\nu\frac{\alpha^2}{\beta^2}\right], \\ w_b(x,y,t) &= W_{bmn}(t)\sin(\alpha x)\sin(\beta y), \\ w_s(x,y,t) &= W_{smn}(t)\sin(\alpha x)\sin(\beta y), \end{aligned} \tag{25}$$

where $W_{mn} = W_{bmn} + W_{smn}, \alpha = m\pi/\alpha,$ and $\beta = n\pi/b.$ The boundary conditions of the present plate model with all edges simply supported are written as [26]:

$$\begin{aligned} x = 0, a:\ & u = \frac{\partial v}{\partial x} = w_b = w_s = \frac{\partial^2 w_b}{\partial x^2} = \frac{\partial^2 w_s}{\partial x^2} = 0, \\ y = 0, b:\ & v = \frac{\partial u}{\partial y} = w_b = w_s = \frac{\partial^2 w_b}{\partial y^2} = \frac{\partial^2 w_s}{\partial y^2} = 0. \end{aligned} \tag{26}$$

The expressions of the displacements in Eq. (25) evidently fulfill all the boundary conditions presented in Eq. (26) as well as the first two equations of motion, Eqs. (21) and (22). By substituting Eq. (25) into Eqs. (23) and (24), we obtain, respectively:

$$\begin{aligned} &\left\{D\left(\alpha^2+\beta^2\right)^2 W_{bmn} + E\left(\alpha^2+\beta^2\right)^2 W_{smn}\right. \\ &+\left[I_0 + I_2\left(\alpha^2+\beta^2\right)\right]\ddot{W}_{bmn} + \left[I_0 + I_4\left(\alpha^2+\beta^2\right)\right]\ddot{W}_{smn} \\ &+\frac{A}{8}W_{mn}^3\left[2\alpha^2\beta^2\nu + \alpha^4\nu^2 + \beta^4\nu^2\right] \\ &\left.+\frac{A}{4}W_{mn}^3\left(1-\nu^2\right)\left[\alpha^4\sin^2(\beta y) + \beta^4\sin^2(\alpha x)\right]\right\} \\ &\cdot\sin(\alpha x)\sin(\beta y) = 0, \end{aligned} \tag{27}$$

$$\begin{aligned} &\left\{E\left(\alpha^2+\beta^2\right)^2 W_{bmn} + \left[F\left(\alpha^2+\beta^2\right)^2 + A^s\left(\alpha^2+\beta^2\right)\right]W_{smn}\right. \\ &+\left[I_0 + I_4\left(\alpha^2+\beta^2\right)\right]\ddot{W}_{bmn} + \left[I_0 + I_5\left(\alpha^2+\beta^2\right)\right]\ddot{W}_{smn} \\ &+\frac{A}{8}W_{mn}^3\left[2\alpha^2\beta^2\nu + \alpha^4\nu^2 + \beta^4\nu^2\right] \\ &\left.+\frac{A}{4}W_{mn}^3\left(1-\nu^2\right)\left[\alpha^4\sin^2(\beta y) + \beta^4\sin^2(\alpha x)\right]\right\} \\ &\cdot\sin(\alpha x)\sin(\beta y) = 0. \end{aligned} \tag{28}$$

By using the Bubnov-Galerkin method:

$$\int_0^a\int_0^b \Lambda\sin(\alpha x)\sin(\beta y)\,dy\,dx = 0, \tag{29}$$

where Λ denotes the left-hand sides of the Eqs. (27) and (28). Then, after performing the double integrations shown in Eq. (29), the following ordinary differential equations can be obtained, respectively:

$$k_{11}W_{bmn} + k_{12}W_{smn} + k_{13}W_{mn}^3 + m_{11}\ddot{W}_{bmn} + m_{12}\ddot{W}_{smn} = 0, \tag{30}$$

$$k_{12}W_{bmn} + k_{22}W_{smn} + k_{13}W_{mn}^3 + m_{12}\ddot{W}_{bmn} + m_{22}\ddot{W}_{smn} = 0, \tag{31}$$

in which

$$\begin{aligned} &k_{11} = D\left(\alpha^2+\beta^2\right)^2, k_{12} = E\left(\alpha^2+\beta^2\right)^2, \\ &k_{13} = \frac{A}{16}\left[4\nu\alpha^2\beta^2 + \left(3-\nu^2\right)\left(\alpha^4+\beta^4\right)\right], \\ &k_{22} = F\left(\alpha^2+\beta^2\right)^2 + A^s\left(\alpha^2+\beta^2\right), \\ &m_{11} = I_0 + I_2\left(\alpha^2+\beta^2\right),\ \ m_{12} = I_0 + I_4\left(\alpha^2+\beta^2\right), \\ &m_{22} = I_0 + I_5\left(\alpha^2+\beta^2\right). \end{aligned} \tag{32}$$

By using the semi-inverse method [32], the variational principles for Eqs. (30) and (31) can be obtained as follows:

$$\begin{aligned} J(W_{bmn}, W_{smn}) = \int_0^{T/4}\Bigg[& k_{12}W_{bmn}W_{smn} + \frac{1}{2}k_{11}W_{bmn}^2 \\ & + \frac{1}{2}k_{22}W_{smn}^2 + k_{13}\left(\frac{1}{4}W_{bmn}^4 + W_{bmn}^3 W_{smn}\right. \\ & \left. + W_{bmn}W_{smn}^3 + \frac{3}{2}W_{bmn}^2 W_{smn}^2 + \frac{1}{4}W_{smn}^4\right) \\ & - m_{12}\dot{W}_{bmn}\dot{W}_{smn} - \frac{1}{2}m_{11}\dot{W}_{bmn} - \frac{1}{2}m_{22}\dot{W}_{smn}^2\Bigg]dt. \end{aligned} \tag{33}$$

The solutions to Eqs. (30) and (31) are obtained by finding $W_{bmn}(t)$ and $W_{smn}(t)$ that make the functional $J(W_{bmn}, W_{smn})$ reaches an extreme. The sinusoidal solutions for $W_{bmn}(t)$ and $W_{smn}(t)$ are approximately presumed as:

$$W_{bmn}(t) = \xi_b\cos(\omega t), W_{smn}(t) = \xi_s\cos(\omega t), \tag{34}$$

where ξ_b and ξ_s are the unknown coefficients, while ω represents the natural frequency of the free vibration of the plate model. After substituting Eq. (34) into Eq. (33), one can obtain:

$$\begin{aligned} J(\xi_b, \xi_s, \omega) = \frac{\pi}{4\omega}\Bigg[& k_{12}\xi_b\xi_s + \frac{k_{11}\xi_b^2}{2} + \frac{k_{22}\xi_s^2}{2} \\ & + \frac{3k_{13}}{16}\left(\xi_b^4 + 4\xi_b^3\xi_s + 6\xi_b^2\xi_s^2 + 4\xi_b\xi_s^3 + \xi_s^4\right) \\ & - \omega^2\left(m_{12}\xi_b\xi_s + \frac{m_{11}\xi_b^2}{2} + \frac{m_{22}\xi_s^2}{2}\right)\Bigg]. \end{aligned} \tag{35}$$

The stationary conditions of the functional $J(\xi_b, \xi_s, \omega)$ read:

$$\frac{\partial J}{\partial \xi_b}=0: k_{11}\xi_b+k_{12}\xi_s+\frac{3}{4}k_{13}\left(\xi_b+\xi_s\right)^3-\omega^2\left(m_{11}\xi_b+m_{12}\xi_s\right)=0, \quad (36)$$

$$\frac{\partial J}{\partial \xi_s}=0: k_{12}\xi_b+k_{22}\xi_s+\frac{3}{4}k_{13}\left(\xi_b+\xi_s\right)^3-\omega^2\left(m_{12}\xi_b+m_{22}\xi_s\right)=0. \quad (37)$$

Let $\xi=\xi_b+\xi_s$ and $\lambda=\xi_b-\xi_s$. The following equation can be obtained after eliminating the variable λ.

$$c_1\omega^4-\left(c_2+c_3\right)\omega^2+\left(c_4+c_5\right)=0, \quad (38)$$

in which

$$c_1=m_{11}m_{22}-m_{12}^2, c_2=k_{11}m_{22}+k_{22}m_{11}-2k_{12}m_{12},$$
$$c_3=\frac{3}{4}k_{13}\xi^2\left(m_{11}+m_{22}-2m_{12}\right), \quad (39)$$
$$c_4=k_{11}k_{12}-k_{12}^2, c_5=\frac{3}{4}k_{13}\xi^2\left(k_{11}+k_{22}-2k_{12}\right).$$

Finally, the nonlinear fundamental natural frequency of the present plate model can be obtained as:

$$\omega_{NL}=\sqrt{\frac{1}{2c_1}\left\{c_2+c_3-\left[\left(c_2+c_3\right)^2-4c_1\left(c_4+c_5\right)\right]^{1/2}\right\}}. \quad (40)$$

When ξ approaches zero or becomes extremely small, the linear fundamental frequency can be expressed as:

$$\omega_L=\sqrt{\frac{1}{2c_1}\left[c_2-\left(c_2^2-4c_1c_4\right)^{1/2}\right]}. \quad (41)$$

4. Numerical results and discussions

In the absence of existing literature on FG nanocomposite plates reinforced by GPLs, conventional FG plates will be utilized for validation purposes, ensuring the accuracy of the solution procedure and the obtained closed-form solutions. A square FG microplate with simply supported boundary conditions is employed to validate the study via the following parameters:

$$E_1=14.4\,GPa, \rho_1=12.2\times10^3\,kg/m^3, E_2=1.44\,GPa,$$
$$\rho_2=1.22\times10^3\,kg/m^3,\ \nu=0.3, h=17.6\times10^{-6}\,m, a/h=10.$$

The dimensionless nonlinear natural frequency $\bar{\omega}$ of the FG microplate is defined as: $\bar{\omega}=\omega_{NL}\left(a^2/h\right)\sqrt{\rho_2/E_2}$. In Table 1, it can be observed that the obtained closed-form solution and the results from the literature are identical for all cases in the selected example.

The parametric study focuses on an FG plate reinforced by GPLs, incorporating the following material properties:

$$Al_2O_3\,(ceramic): E_1=380\,GPa,\ \rho_1=3800\,kg/m^3,$$
$$Al\,(metal): E_2=70\,GPa,\ \rho_2=2702\,kg/m^3,$$
$$GPL: E_{GPL}=1.01\,TPa,\ \rho_{GPL}=1062.5\,kg/m^3, \quad (42)$$
$$t_{GPL}=1.5\,nm,\ w_{GPL}=1.5\,\mu m,\ l_{GPL}=2.5\,\mu m.$$

The Poisson's ratio is taken as $\nu=0.3$. Otherwise stated, the normalized nonlinear frequency of the FG plate is defined as $\bar{\omega}_{NL}=\omega_{NL}\left(a^2/h\right)\sqrt{\rho_1/E_1}$. The impact of the GPL weight fraction, varying from 0 to 1.5%, on the relative change of the nanocomposite plate's natural frequency are shown in Fig. 3. The relative change of the natural frequency is defined as the percentage change in frequency compared to the frequency of the plate without GPL reinforcement. It can be observed that increasing the amount of GPLs leads to an increased relative frequency change in all cases. In addition, it is clear that the GPL dispersion pattern D results in the highest natural frequency, followed by pattern A. Conversely, the GPL dispersion pattern C provides the lowest natural frequency. In detail, incorporating GPL into the constituent material with lower stiffness and concentration of the reinforcement closer to the plate's top and bottom surfaces demonstrates greater effectiveness in increasing the natural frequency compared to those concentrated near the mid-plane.

Fig. 4 investigates the impact of vibration amplitude on the nonlinear frequency ratio ω_{NL}/ω_L of the plate model across various GPL patterns. The parameters used in this analysis are $W_{GPL}=1\%, N=1,$ and mode $(m,n)=(1,1)$. The findings indicate that as the vibration amplitude of the plate model increases, the natural frequency ratio also increases. This signifies a growing disparity between considering and neglecting the nonlinearity in the system. It should be noted that, in contrast to the findings regarding the nonlinear natural frequency, the GPL patterns A and D exhibit the lowest nonlinear frequency ratio across the entire range of vibration amplitudes. This suggests that this particular combination is more effective in minimizing the influence of nonlinearity on the plate's frequency response.

Table 1 Comparison of nonlinear natural frequency $\bar{\omega}$ of a simply supported square FG microplate.

N	Results	ξ/h					
		0	0.2	0.4	0.6	0.8	1
1	Ref. [26]	5.2698	5.4126	5.8201	6.4423	7.2239	8.119
	Present	5.2698	5.4126	5.8201	6.4423	7.2239	8.119
5	Ref. [26]	5.5351	5.6711	6.0609	6.6601	7.4181	8.2915
	Present	5.5351	5.6711	6.0609	6.6601	7.4181	8.2915
10	Ref. [26]	6.1157	6.2388	6.5943	7.1476	7.8571	8.6845
	Present	6.1157	6.2388	6.5943	7.1476	7.8571	8.6845

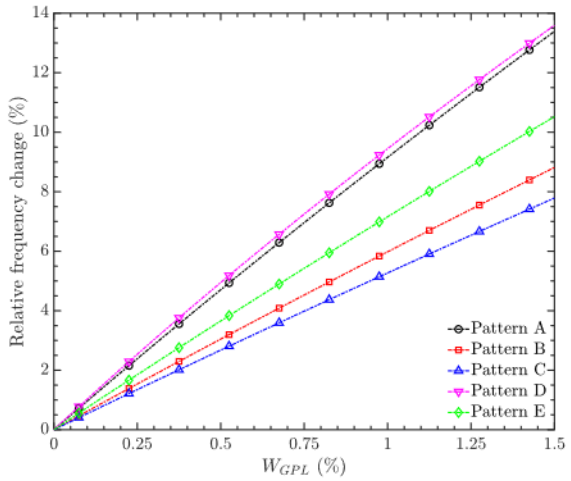

Fig. 3 Influence of GPL weight fraction on the relative change of natural frequency

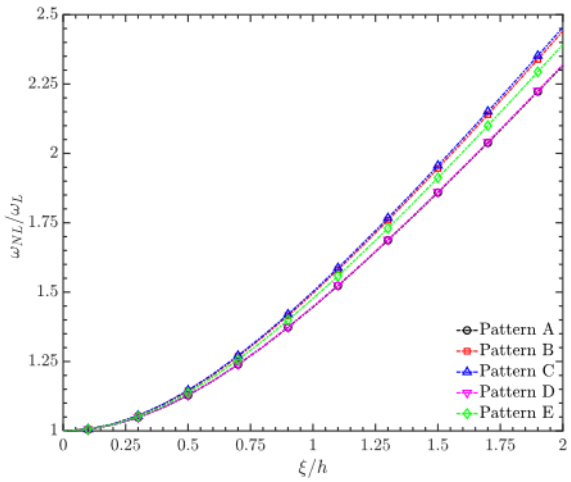

Fig. 4 Influence of vibration amplitude on the nonlinear frequency ratio for various matrix gradations and GPL patterns.

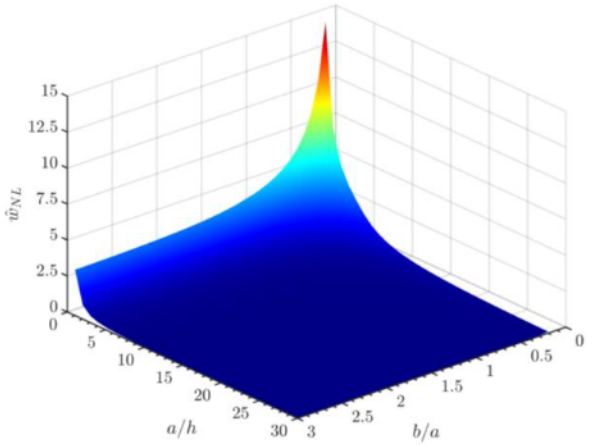

Fig. 5 Influence of aspect ratio and length-to-thickness ratio on the normalized natural frequency.

To demonstrate the impacts of the aspect ratio b/a and length-to-thickness ratio a/h of the plate model on the normalized natural frequency $\hat{\omega}_{NL} = \omega_{NL} h\sqrt{\rho_1 / E_1}$, the nanocomposite plate with the GPL pattern D is employed. The chosen parameters for the plate model are as follow: $W_{GPL} = 1\%, N = 1, \xi / h = 1,$ and mode $(m,n) = (1,1)$. Fig. 5 shows that as the length-to-thickness ratio a/h and aspect ratio b/a increase, the natural frequency of the plate decreases.

5. Conclusions

The nonlinear free vibration analysis of the nanocomposite plate consisting of FG matrix reinforced by GPLs was conducted. The study examined five different GPL distribution patterns (patterns A, B, C, D, and E). The equations of motion of the plate were developed and solved utilizing the RPT, von Karman's nonlinearity, Hamilton's principle, the Bubnov-Galerkin method, and a variational approach. The main conclusions from the results can be described as follows: (1) the addition and pattern of GPL distribution significantly affect the nonlinear natural frequency of the nanocomposite plate; (2) GPL dispersion pattern D results in the highest natural frequency, while the dispersion pattern C provides the lowest natural frequency; (3) increasing the GPL weight fraction leads to an increased relative frequency change in all cases; (4) the impact of vibration amplitude shows that as the vibration amplitude of the plate model increases, the natural frequency ratio ω_{NL} / ω_L also increases; (5) with increasing aspect ratio b/a and length-to-thickness ratio a/h, the natural frequency of the nanocomposite plate decreases.

References

[1] Koizumi, M., *FGM activities in Japan.* Composites Part B: Engineering, 1997. **28**(1-2): p. 1-4.

[2] Zhao, S., et al., *Functionally graded graphene reinforced composite structures: A review.* Engineering Structures, 2020. **210**: p. 110339.

[3] Praveen, G. and J. Reddy, *Nonlinear transient thermoelastic analysis of functionally graded ceramic-metal plates.* International journal of solids and structures, 1998. **35**(33): p. 4457-4476.

[4] Dinh Duc, N., et al., *Nonlinear dynamic response and vibration of imperfect shear deformable functionally graded plates subjected to blast and thermal loads.*

Mechanics of Advanced Materials and Structures, 2017. **24**(4): p. 318-329.

[5] Huang, X.-L. and H.-S. Shen, *Nonlinear vibration and dynamic response of functionally graded plates in thermal environments.* International Journal of Solids and Structures, 2004. **41**(9-10): p. 2403-2427.

[6] Wang, Y.Q. and J.W. Zu, *Large-amplitude vibration of sigmoid functionally graded thin plates with porosities.* Thin-Walled Structures, 2017. **119**: p. 911-924.

[7] Woo, J., S. Meguid, and L. Ong, *Nonlinear free vibration behavior of functionally graded plates.* Journal of sound and vibration, 2006. **289**(3): p. 595-611.

[8] Abdulkerim, S., A. Dafnis, and H.-G. Riemerdes, *Experimental investigation of nonlinear vibration of a thin rectangular plate.* International Journal of Applied Mechanics, 2019. **11**(06): p. 1950059.

[9] Kuilla, T., et al., *Recent advances in graphene based polymer composites.* Progress in polymer science, 2010. **35**(11): p. 1350-1375.

[10] Lau, A.K.-T. and D. Hui, *The revolutionary creation of new advanced materials—carbon nanotube composites.* Composites Part B: Engineering, 2002. **33**(4): p. 263-277.

[11] Soni, S.K., et al., *Functionally graded carbon nanotubes reinforced composite structures: An extensive review.* Composite Structures, 2022: p. 116075.

[12] Geim, A.K. and K.S. Novoselov, *The rise of graphene.* Nature materials, 2007. **6**(3): p. 183-191.

[13] Huang, X., et al., *Graphene-based composites.* Chemical Society Reviews, 2012. **41**(2): p. 666-686.

[14] Liu, J., H. Yan, and K. Jiang, *Mechanical properties of graphene platelet-reinforced alumina ceramic composites.* Ceramics International, 2013. **39**(6): p. 6215-6221.

[15] Li, S., et al., *Enhanced strength and toughness of silicon carbide ceramics by graphene platelet-derived laminated reinforcement.* Journal of Alloys and Compounds, 2020. **834**: p. 155252.

[16] Liu, J., et al., *Preparation and mechanical performance of graphene platelet reinforced titanium nanocomposites for high temperature applications.* Journal of Alloys and Compounds, 2018. **765**: p. 1111-1118.

[17] Li, K., et al., *Isogeometric analysis of functionally graded porous plates reinforced by graphene platelets.* Composite Structures, 2018. **204**: p. 114-130.

[18] Song, M., S. Kitipornchai, and J. Yang, *Free and forced vibrations of functionally graded polymer composite plates reinforced with graphene nanoplatelets.* Composite Structures, 2017. **159**: p. 579-588.

[19] Bellifa, H., et al., *Bending and free vibration analysis of functionally graded plates using a simple shear deformation theory and the concept the neutral surface position.* Journal of the Brazilian Society of Mechanical Sciences and Engineering, 2016. **38**: p. 265-275.

[20] Farzam-Rad, S.A., B. Hassani, and A. Karamodin, *Isogeometric analysis of functionally graded plates using a new quasi-3D shear deformation theory based on physical neutral surface.* Composites Part B: Engineering, 2017. **108**: p. 174-189.

[21] Lou, J. and L. He, *Closed-form solutions for nonlinear bending and free vibration of functionally graded microplates based on the modified couple stress theory.* Composite Structures, 2015. **131**: p. 810-820.

[22] Zhang, D.-G., *Modeling and analysis of FGM rectangular plates based on physical neutral surface and high order shear deformation theory.* International Journal of Mechanical Sciences, 2013. **68**: p. 92-104.

[23] Zhang, D.-G. and Y.-H. Zhou, *A theoretical analysis of FGM thin plates based on physical neutral surface.* Computational Materials Science, 2008. **44**(2): p. 716-720.

[24] Roun, S., V.-L. Nguyen, and J. Rungamornrat, *Free Vibration and Buckling Analyses of Functionally Graded Plates with Graphene Platelets Reinforcement.* Journal of Computing and Information Science in Engineering, 2024: p. 1-44.

[25] Tjong, S.C., *Recent progress in the development and properties of novel metal matrix nanocomposites reinforced with carbon nanotubes and graphene nanosheets.* Materials Science and Engineering: R: Reports, 2013. **74**(10): p. 281-350.

[26] Lou, J., et al., *Nonlinear analyses of functionally graded microplates based on a general four-variable refined plate model and the modified couple stress theory.* Composite Structures, 2016. **152**: p. 516-527.

[27] Mechab, I., B. Mechab, and S. Benaissa, *Static and dynamic analysis of functionally graded plates using four-variable refined plate theory by the new function.* Composites Part B: Engineering, 2013. **45**(1): p. 748-757.

[28] Zhang, D.-G., *Nonlinear bending analysis of FGM beams based on physical neutral surface and high order shear deformation theory.* Composite Structures, 2013. **100**: p. 121-126.

[29] Emam, S.A. and A.H. Nayfeh, *Postbuckling and free vibrations of composite beams.* Composite Structures, 2009. **88**(4): p. 636-642.

[30] Emam, S.A., *A static and dynamic analysis of the postbuckling of geometrically imperfect composite beams.* Composite Structures, 2009. **90**(2): p. 247-253.

[31] Niyogi, A., *Nonlinear bending of rectangular orthotropic plates.* International Journal of Solids and Structures, 1973. **9**(9): p. 1133-1139.

[32] He, J.-H., *Variational principles for some nonlinear partial differential equations with variable coefficients.* Chaos, Solitons & Fractals, 2004. **19**(4): p. 847-851.